TWO-DIMENSIONAL CUSPED INTERFACES

Daniel D. Joseph and John Nelson

Department of Aerospace Engineering and Mechanics
University of Minnesota
110 Union Street SE
Minneapolis, MN 55455

Michael Renardy and Yuriko Renardy

Department of Mathematics and ICAM
Virginia Polytechnic Institute and State University
Blacksburg, VA 24061-0123

To appear in the *Journal of Fluid Mechanics*
(in press)

Two-dimensional cusped interfaces are line singularities of curvature. We create such cusps by rotating a cylinder half immersed in liquid. A liquid film is dragged out of the reservoir on one side and is plunged in at the other, where it forms a cusp at finite speeds, if the conditions are right. Both Newtonian and non-Newtonian fluids form cusps, but the transition from a rounded interface to a cusp is gradual in Newtonian liquids and sudden in non-Newtonian liquids. We present an asymptotic analysis near the cusp tip for the case of zero surface tension, and we make some remarks about the effects of a small surface tension. We also present the results of numerical simulations showing the development of a cusp. In those simulations, the fluid is filling an initially rectangular domain with a free surface on top. The fluid enters from both sides and is sucked out through a hole in the bottom.

1. Introduction

Our photographs were produced in a four roll mill apparatus of the type introduced by G.I. Taylor to study the deformation of drops and bubbles in a pure straining flow. We built the apparatus with the same purpose in mind, but first put the cylinders into rotation in a partially filled apparatus whose configuration and orientation relative to gravity are obvious from the photographs. As a result, we discovered the rollers which were described by Joseph, Nguyen and Beavers [1984].

At that time, we noticed another entirely different flow regime, the two-dimensional cusped interfaces which we shall describe in this paper. At this point, we ask the reader to inspect the photographs. They show cusped, two-dimensional interfaces. No rounding can be detected, at least not on a visible length scale.

S. Richardson [1968] did an elegant analysis of two-dimensional bubbles in Stokes flow. He proved that the only possible line singularity of the interface between a viscous liquid and an inviscid two-dimensional bubble is a true cusp. For a cusp that opens on the negative x-axis, his expression for the leading contribution to the stream function, expressed in polar coordinates, is

$$\psi = \frac{\sigma}{2\pi\mu}\, r \log r \sin\phi \tag{1}$$

Here σ is the surface tension coefficient and μ is the viscosity. This formula shows that there is a point force 2σ exerted by the free surface on the fluid and that the velocity near the origin is in the negative x-direction. The velocity near the origin is infinite and, perhaps more seriously, the velocity gradient is not square integrable, leading to an infinite amount of energy dissipation. The free surface at leading order simply coincides with the negative x-axis; the actual opening of the cusp would have to be determined from higher order corrections which are worked out here at lowest order.

Lamb [1932, p. 607] derived (1) for the problem of a point force acting at the center of a circle and he notes that the solution "… fails to give a definite result …" as the radius of the

circle tends to infinity. In our problem, (1) arises from a local analysis near the cusp, and the behavior for large r is irrelevant. However, there are also physical difficulties associated with (1) for very small r on which we comment below. We shall regard (1) as valid in an intermediate range, where r is small compared to geometric lengthscales of the problem, but nevertheless log $r^{\sigma/2\pi\mu}$ cannot be regarded as "large."

Evidently the main features of our experiments cannot be explained in terms of (1), since the velocity of the fluid is in the positive, rather than the negative, x-direction, as shown in Figure 1. Moreover, the deviation of the interface from a flat surface, neglected by Richardson, is clearly an important feature of the experiments. The experiments also suggest that, although cusped free surfaces can appear in Newtonian fluids, they are easier to create in non-Newtonian fluids. The cusp does not appear at the slowest speeds; it forms more gradually in Newtonian than in non-Newtonian fluids. This is reminiscent of the transition from rounded to pointed ends in the bubble experiments of Rumscheidt and Mason [1961].

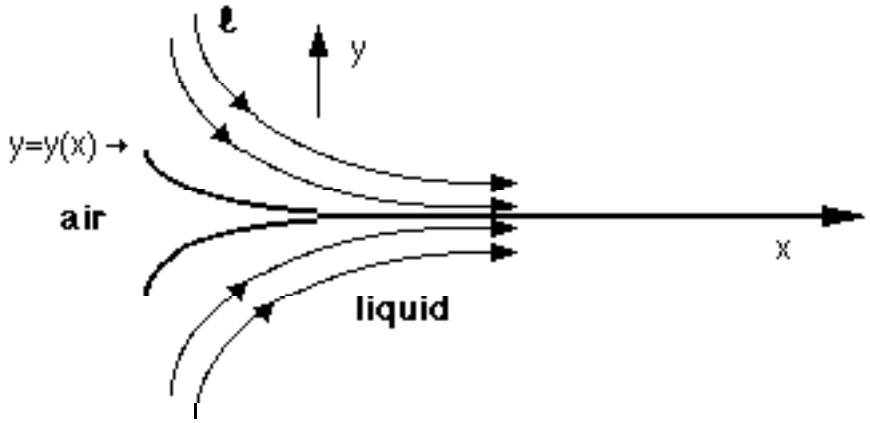

Figure 1. Flow past a cusp.

Our analysis takes a different point of view from Richardson's. We first analyze the local behavior near a cusp singularity in the absence of surface tension. In this case, we find an interface shape given at leading order by $y^2 = -cx^3$ for Newtonian and linear viscoelastic fluids. The stresses at the cusp in a linear viscoelastic fluid are less singular than in a Newtonian fluid. On the other hand, nonlinear effects in viscoelastic fluids are probably important near the stagnation point that must be present on a smooth interface. The build-up of extensional stresses

near such a stagnation point is likely to favor cusping. In the presence of surface tension, our analysis is not valid close to the tip of the cusp, where the leading contribution (if there is a true cusp) should be given by Richardson's solution. As a measure of the importance of Richardson's solution, we calculate where the magnitude of the resulting velocity would be comparable to that of the macroscopically observed flow. For the surface tension parameters involved in the experiments, this is the case only at extremely small length scales, extending beyond the limits of the validity of Laplace's theory of surface tension. The issue was addressed by Lord Rayleigh [1890], who notes that "… the walls of a moderately small cavity certainly tend to collapse with a force measured by the constant surface tension of the liquid. The pressure in the cavity is first proportional to the surface tension and to the curvature of the walls. If this law held without limit, the consideration of an infinitely small cavity shows that the intrinsic pressure would be infinite in all liquids. Of course, the law really changes when the dimensions of the cavity are of the same order as the range of attractive forces, and the pressure in the cavity approaches a limit." We therefore believe that surface tension plays no major role in the experimentally observed flows and that the analysis given here describes the main features.

Richardson's result and ours may have some relevance for pointed bubbles, which are point singularities of the curvature. Such singularities have been described by Taylor [1934], Rumscheidt and Mason [1961], Taylor [1964], Grace [1971], Buckmaster [1972,1973], Acrivos and Lo [1978], Rallison and Acrivos [1978], Hinch and Acrivos [1979], and Sherwood [1981] for the case of Newtonian fluids. Buckmaster is the only author in this list who discussed Richardson's results. He comments that Richardson has "… shown that such discontinuities, if they exist, must be genuine cusps …" He also expresses reservations about the relevance of two-dimensional cusps: "On the one hand it is doubtful that pointed two-dimensional drops could be stable, and on the other there is a point force associated with corners—which a three-dimensional drop would not generate." These remarks appear to have halted further consideration of two-dimensional cusps.

The existence of point singularities for axisymmetric bubbles in Newtonian fluids and the decision about whether these might be corner or cusped singularities still seems not to have been decided.

There is a marked difference between the shape of air bubbles rising in Newtonian and non-Newtonian liquids, with a much stronger tendency toward cusping in the non-Newtonian case (see Figure 2).

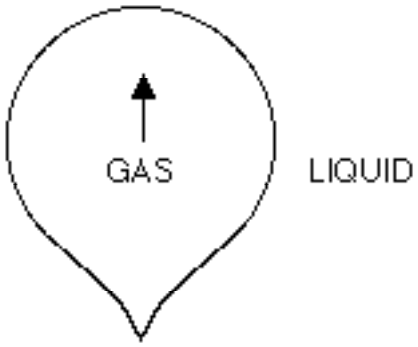

Figure 2. Gas bubble rising in a non-Newtonian liquid. Bubbles rising in Newtonian liquids do not tail. The shape of the bubble depends strongly on the bubble volume.

The flow at the trailing edge of a rising gas bubble is in a rough way analogous to flow near the cusp in our experiments, though there are obvious and perhaps not so obvious differences between streaming around axisymmetric and plane cusps. The tail shown in Figure 2 occurs only in non-Newtonian liquids and has been reported in experiments by Phillippoff [1937], Warshay, Bogusz, Johnson and Kintner [1959], Mhatre and Kintner [1959], Astarita and Apuzzo [1965], Barnett, Humphrey and Litt [1966], Calderbank [1967], Calderbank, Johnson and Loudon [1970], Leal, Skoog and Acrivos [1971] and Zana and Leal [1978]. Again, it is not certain that the tail can form a true cusp. Astarita and Apuzzo note that "The bubble is … unexpected; it is clearly prolate and the lower pole is markedly cuspoidal." Hassager [1985] reports experiments where the bubble is not axisymmetric but flattened; it appears to have a straight edge at the trailing end.

We present our experimental results in the following section. Section 3 contains the local analysis of fluid behavior near a cusp. In Section 4, we show some numerical simulations using

the FIDAP package. The flow there involves a fluid entering from both the right and left and bounded by a free surface on top. The fluid is being sucked downward. The numerical results are consistent with the interpretation that a singularity in the free surface is developing if the surface tension is small enough. For larger values of surface tension, a steady state with a smooth interface is reached instead. The final section of the paper gives a summary of the results.

2. Experiments

Two equal cylinders whose centerlines lie in the same plane z=const., perpendicular to gravity, are immersed in liquid approximately up to their centerline. Then the cylinders are put into counter rotation with the same speed. There are two possibilities; the liquid is drawn up at the outside of the cylinders and forced down in the center, or vice versa, as in Figure 3. Typically more than half of each cylinder is coated with a liquid of relatively uniform thickness. The thickness and covering of the arc of the coating liquid depends on the viscosity of the liquid and the speed of the cylinder.

Cusps form in some liquids and not in others. Once a cusp forms it will persist and sharpen as the angular velocity is increased. Some liquids with sharp cusps are exhibited in Figures 3 through 11. Liquids which do not cusp have clearly rounded ends as in Figure 7(b). Tables 1 and 2 list fluids which form cusps and Table 3 lists fluids which do not cusp at the angular speeds we attained. The fluids that do eventually cusp apparently do not do so at the slowest speed (see figures 8 through 15). It therefore appears that cusping is a threshold phenomenon characterized by a threshold parameter which in our experiments is a critical value of the angular velocity of the cylinders. Some specific values of this critical speed are given in the figure captions; to convert this rotation speed into a linear speed one has to multiply by the observed radius at the point of cusping which is slightly larger (Table 4) than the radius 1.25 cm of the cylinder. For non-Newtonian fluids, the critical value of the rotation speed is very distinct. Below this value the interface is round. At the critical speed the interface suddenly transforms to a cusp. The critical speed is not distinct for those Newtonian fluids for which a cusp was observed. At slow rotation speeds the interface is round. As the rotation speed increases, the

shape of the interface changes from rounded to pointed in a continuous manner, until at what we define as the critical speed the interface appears to be a cusp. Once a cusp is formed, further increases in the angular velocity will only sharpen the cusp or end in an instability characterized by fingering.

The liquids listed in Table 1 which do form apparently unambiguous cusps are non-Newtonian. They have non-zero normal stress differences and they all climb rotating rods. At the same time, these fluids are on the average more viscous than the Newtonian liquids which do, and those which do not, form cusps and are listed in Tables 2 and 3. We tested the liquids in Tables 2 and 3 and none of them will climb a rotating rod. Newtonian fluids which are too mobile will not cusp at the speeds we could attain in our apparatus and may never cusp because of turbulence.

Fluid	Viscosity (p)	Density (g/cm^3)	Surface Tension (dyn/cm)
1% Aqueous Polyox	61.2	1.000	48.4
2% Aqueous Polyox	600	1.125	44.4
M1	30.0	0.859	29.9
Silicone Oil—12500cs	122	0.975	21.5
STP	143	0.858	35.0
TLA 510	220	0.868	31.1
Honey	109	1.40	69.3

Table 1. Representative values of the viscosity and surface tension of cusping non-Newtonian liquids at temperatures in the neighborhood of 23° C.

Fluid	Viscosity (p)	Density (g/cm^3)	Surface Tension (dyn/cm)
Castor Oil	8.15	0.960	35.1
Glycerin	8.30	1.265	63.3
Silicone Oil—500cs	4.86	0.971	21.1
Silicone Oil—1000cs	9.71	0.971	21.2
Silicone Oil—5000cs	48.6	0.971	21.3

Table 2. Representative values of the viscosity and surface tension of cusping Newtonian liquids at temperatures in the neighborhood of 23° C.

Fluid	Viscosity (p)	Density (g/cm^3)	Surface Tension (dyn/cm)
SAE 30 Motor Oil	2.80	0.886	35.0
Safflower Oil	0.469	0.920	23.0
Silicone Oil—200cs	1.94	0.970	21.0
Soybean Oil	0.489	0.922	25.7

Table 3. Representative values of the viscosity and surface tension of Newtonian liquids that do not cusp at temperatures in the neighborhood of 23° C.

We measured the critical value of the angular velocity of the cylinders for the transition from rounded to cusped ends in a number of liquid-air systems and in the two-liquid SAE 30 motor oil and water system shown in Figure 8. A dimensionless capillary number was calculated by the formula $Ca=\mu U/\sigma$, where μ is the viscosity, σ the surface tension coefficient, and an estimate for the velocity U is ωr, where ω is the angular speed of the cylinder and r is the radius of the fluid at the cusp point. The value of Ca for SAE 30-water was computed using a surface tension constant of 9.22 dyn/cm; the surface tension constant tabulated above is for SAE 30 against air.

System	Critical Angular Velocity (RPM)	Critical Radius (cm)	Ca_c
Newtonian Fluids:			
Castor Oil	113	1.78	4.89
Glycerin	128	1.49	2.62
Silicone Oil—500cs	75	1.64	2.96
Silicone Oil—1000cs	41	1.40	2.75
Silicone Oil—5000cs	26	1.57	8.21
SAE 30 Motor Oil—Water	51	1.61	2.57
Non-Newtonian Fluids:			
Honey	5.58	1.92	1.78
Polyox (1%)	52	1.35	9.24
Polyox (2%)	0.8	1.97	2.10
Silicone Oil—12500cs	3.0	1.50	2.64
M1	2.4	1.90	0.48
STP	2.9	1.80	2.24

Table 4. Critical annular velocity and Ca_c values for the formation of a cusp.

For all Newtonian fluids, the measured values of Ca_c are in excess of 2.5. Some non-Newtonian fluids lead to lower values of Ca_c**.** However, this appearance may be deceiving. The "viscosity" used in computing Ca is the zero shear rate viscosity. The flows studied here are likely to involve significant extensional motion, and extensional viscosities of non-Newtonian fluids increase substantially with the rate of extension.

We tried to obtain two-dimensional cusped interfaces in a number of two-liquid systems. In general we do not expect to achieve cusped interfaces in two-liquid systems; the dynamics which would lead to a cusp in air will give rise to a fingering flow or rollers in a two-liquid system. In many of these two-liquid systems, rollers and fingering flows were described already by Joseph, Nguyen and Beavers [1984]. Rollers form when one of the two fluids is much more viscous than the other. For example, rollers form in STP-water and silicone oil-water systems with oils in excess of 1000p. Therefore, fluids like 12500 cs silicone oil, STP and TLA 510 which give rise to cusps in air lead to rollers in water. On the other hand, 100 cs silicone oil in water gives rise to the fingering of water into silicone oil at higher speeds and not to rollers.

For lower viscosity liquids the interface remains smooth at low speeds, while at higher speeds one liquid will finger into the other. In thinking about this, it is useful to imagine how the streamlines would look at a nearly cusped smooth surface. This is sketched in Figure 17. It is clear that the nose of the interface must be a stagnation point if the interface is not cusped. The internal motion of the fluid inside the nose is yet more complicated. It is being dragged toward the nose near the interface and must either be turned around by the pressure at the stagnation point into the double eddy or else finger into the fluid outside the nose. At higher speeds both these possibilities are realized intermittently.

There are evidently some pairs of liquids for which cusp solutions can be realized. One of these, motor oil and water, is shown in Figure 8. This cusped surface is not two-dimensional, but scalloped. The crests of the scallops are fingering sites for small water bubbles to enter the oil. The scalloping is a fairly common feature and it can be seen in the M1-air interface shown in Figure 6b. At higher speeds the air at a cusped interface fingers into the liquid at these sites. Fingering always appears at scallop sites, really by definition because the scallop is what remains after the bubble has broken away. This kind of fingering leads to emulsions (cf. Section 5.3 in Joseph, Nguyen and Beavers [1984]).

Figure 17. Distorted interface in a two-liquid system. The point A is a stagnation point or a cusp. When $\Omega=0$, each fluid covers one-half of the cylinder. We do not know which fluid will finally be on the rod. There is nothing in our equations to tell us; contact angles are not enough.

3. Theory

We are going to assume that there is a cusp at the origin of the x,y-plane as shown in Figure 1.

The flow is assumed to be a small perturbation of uniform flow with velocity U in the positive x-direction, and the free surface is a small perturbation of the negative x-axis. Let (u,v) denote the perturbations to the velocity and let h denote the position of the free surface that is located above the cusp. We first analyze Newtonian fluids with zero surface tension. We introduce a stream function ψ by

$$u = \psi_y, \; v = -\psi_x \; . \tag{2}$$

The positive x-axis is a line of symmetry, we first look for antisymmetric stream functions, corresponding to symmetric flow fields. In polar coordinates, we then have the following expression for the stream function (cf. Dean and Montagnon [1949], Michael [1958])

$$\psi = r^{\lambda}[A \sin(\lambda\phi) + B \sin((\lambda-2)\phi)] \; ; \tag{3}$$

this expression incorporates the desired symmetry. At $\phi=\pi$, we must satisfy the conditions of zero shear and normal stress,

$$u_y + v_x = 0, \; 2\mu v_y - p = 0 \; , \tag{4}$$

which can be shown to translate into

$$\frac{1}{r^2}\,\psi_{\phi\phi} + \frac{1}{r}\,\psi_r - \psi_{rr} = 0 \; ,$$

$$\frac{3}{r}\,\psi_{rr\phi} + \frac{1}{r^3}\,\psi_{\phi\phi\phi} - \frac{3}{r^2}\,\psi_{r\phi} + \frac{4}{r^3}\,\psi_{\phi} = 0 \; . \tag{5}$$

We may evaluate (5), using (3), and we find that

$$[\lambda A + (\lambda-2)B] \sin(\lambda\pi) = 0 \; ,$$

$$(A+B)\cos(\lambda\pi) = 0 . \tag{6}$$

Clearly, we have nontrivial solutions for $\lambda=3/2$. The linearization of the kinematic free surface condition leads to

$$Uh' = v = -\psi_x = \psi_r , \tag{7}$$

and hence

$$h = \frac{1}{U} r^{\lambda} (A+B). \tag{8}$$

Symmetric stream functions (i.e. antisymmetric flows) are given by the expression

$$\psi = r^{\lambda}[A\cos(\lambda\phi) + B\cos((\lambda-2)\phi)] . \tag{9}$$

In this case, (5) leads to

$$[\lambda A + (\lambda-2)B]\cos(\lambda\pi) = 0 ,$$

$$(A+B)\sin(\lambda\pi) = 0 . \tag{10}$$

Again, $\lambda=3/2$ is a solution; in place of (8) we get $h=0$.

Hence, if surface tension is neglected, cusped solutions with $h \sim r^{3/2}$ are possible. Figure 16 compares measured values of the cusp tip with $y=-cx^{3/2}$. This type of comparison between theory and experiment is only qualitative since we don't know c or the values of x for which the higher order corrections become important. The higher order corrections would be a composition of symmetric and antisymmetric functions like (3) and (9) in a combination determined globally.

Now, let us consider what happens if surface tension is included. Then we must change several things. First, we must include a term $\frac{\sigma}{\mu U} \psi_{rrr}$ on the right hand side of the normal stress condition (5); this term arises if we reexpress h'' using (7). This changes the second part of equation (6) to

$$(A+B)\left[2\cos(\lambda\pi) - \frac{1}{Ca}\sin(\lambda\pi)\right] = 0 \,. \tag{11}$$

Hence λ becomes the root of $\tan(\lambda\pi)=2Ca$, which approaches 3/2 as $Ca \varnothing \infty$. (In the antisymmetric case, we still find $\lambda=3/2$ and $h=0$.) Second, the solution (1) cannot be valid all the way up to the cusp. This is because at the cusp the angle of the interface has a jump of 2π, leading to a delta function singularity in the traction. This point force must be balanced by a singularity in the flow. This consideration led to Richardson's [1968] solution (1), which may be written as

$$r \log (r^{\sigma/2\pi\mu}) \sin\phi \,. \tag{12}$$

The velocity resulting from (12) has a logarithmic singularity at the cusp; the assumption of small perturbation of uniform flow on which the preceding analysis was based is thus rendered invalid. The velocity gradient resulting from (12) is not square integrable and thus there would be an infinite amount of energy dissipation. This raises questions about the physical realizability of a solution such as (12).

On the other hand, in order for the velocity from (12) to be of the same order as U, we must have $\log r \sim 2\pi Ca$. Here it is understood that r is made dimensionless by a geometric lengthscale. These scales are the only ones available for Stokes flow in which U, σ and μ are the material parameters. The density cannot enter into this list. We must have a Stokes flow locally near the cusp singularity where highest derivatives are ever more dominant. In fact, even globally the Reynolds number based on cylinder diameter and speed in never greater than one and is usually orders of magnitude smaller than one. A convenient geometric lengthscale is the distance to the cusp point, slightly larger than the cylinder radius, 1.25 cm. Using 2.5 as a lower bound for Ca, we find that log r must be on the order of 15.7. From this we conclude that Richardson's solution does not dominate over the macroscopic (approximately uniform) flow until we reach a lengthscale of approximately 10^{-7} cm, 10 Ångstroms. Such lengthscales are far beyond the means of optical observation and actually reach the limits of applicability of continuum mechanics. Van der Waals forces across the air gap between the long arcs at the cusp can be expected to become

important already at 1000 Å and the physics of disjoining pressures would then be important long before Richardson's solution acts strongly. It thus appears reasonable to assume that the physical difficulties posed by Richardson's solution are resolved at the molecular level. However these questions may ultimately be resolved at the molecular level, we may regard Richardson's solution, which has dimensionless velocities proportional to log $r^{\sigma/2\pi\mu}$, as valid on observable lengthscales with r, dimensionless say with the cylinder radius a=1.25 cm, of order one or less. Clearly on these lengthscales, the velocities log $r^{\sigma/2\pi\mu}$ are not "large," they are small, and our analysis based on perturbing uniform flow is at least qualitatively valid. Richardson's expression (12) is a solution and it satisfies all the required interface conditions on the unperturbed interface, but is effectively unobservable at the intermediate scales at which (9) holds.

The issue of a singularity at the free surface might be made clearer by a comparison to the analogous contact line problem. There, one often observes a fluid-fluid-solid contact line moving steadily, while the local analysis based on the Stokes equations and the usual boundary conditions (Huh and Scriven [1971]) predicts a singular stress tensor and energy dissipation. The singularity found by Huh and Scriven arises from a stream function proportional to r and it gives rise to a 1/r singularity in the stress and a logarithmic singularity in the force. Richardson's singular solution (1) or (12) is slightly more singular than this and our intermediate singular expression (9) is slightly less singular. Subsequent theoretical work (e.g., Dussan [1976], de Gennes [1985], and earlier papers cited therein) indicates that the singular solution should be regarded as valid at intermediate scales, and that a number of microscopic mechanisms (slip at high stress, precursor films, disjoining pressures, roughness, …) can remove the singularity with no macroscopically discernible effect. In the worst possible case, the singularity is removed by a breakdown of the no slip condition at the molecular scale (Koplick, Banavar and Willemson [1988], Thompson and Robbins [1989]).

We conclude this section with some remarks about viscoelastic fluids. Let us first consider a linear viscoelastic fluid; we assume zero surface tension. In this case, the Newtonian

velocity field given above actually provides a solution even for the viscoelastic case; the stresses, however, are now given by

$$\mathbf{T}(x,y) = \int_0^\infty G(s)\mathbf{D}(x-Us,y)\, ds\,, \tag{13}$$

where G denotes the stress relaxation function and D the symmetric part of the velocity gradient. We note that the stresses given by (13) would be less singular at the cusp than in the Newtonian case. On the other hand, if we use the second order fluid approximation, $\mathbf{T}=\mu\mathbf{D}+\alpha_1 U\frac{\partial \mathbf{D}}{\partial x}$, where $\mu=\int_0^\infty G(s)ds$, $\alpha_1=-\int_0^\infty sG(s)ds$, then the stresses for a given velocity field are more singular than in the Newtonian case. The second order fluid cannot be a valid approximation close to the cusp, but it may be valid some distance away from the cusp.

It appears doubtful whether linear viscoelasticity is very useful in interpreting experiments in non-Newtonian fluids. The extensional behavior of such fluids is highly nonlinear, leading to extensional stresses much larger than those in Newtonian fluids with the same shear viscosity. We note that a non-cusped interface necessarily has a stagnation point, with the associated potential for a build-up of elongational stresses. Cusping gets rid of the stagnation point and alleviates some of these elongational stresses. This effect should favor cusping in non-Newtonian fluids. The behavior of non-Newtonian fluids at cusps and in general at corners larger than 180° is not well understood (see Davies [1988] for some partial results).

We do not understand the mechanism leading to a critical capillary number even in the Newtonian case. For non-Newtonian fluids, more dimensionless quantities can be formed, in addition to the capillary number introduced above. The critical capillary numbers displayed in Table 4 are of the same order of magnitude for non-Newtonian as for Newtonian fluids, but there is a definite trend to lower capillary numbers in the non-Newtonian case. To rectify this, one may think of replacing the Newtonian viscosity in the definition of Ca by some non-Newtonian viscosity. We note that the extensional viscosity of non-Newtonian fluids generally increases

with elongation rate, so that such a procedure would give higher capillary numbers if we think of the flow as being primarily extensional. We give an alternative dimensional analysis based on the second order fluid. For this we estimate elongational stresses as $|\alpha_1|U^2/\ell^2$, where ℓ is a characteristic length, and we estimate stresses resulting from surface tension as σ/ℓ. This leads to the capillary number $Ca=|\alpha_1|U^2/\sigma\ell$. Next we estimate ℓ as $U\tau$, where τ is a characteristic time scale, so we have $Ca=|\alpha_1|U/\sigma\tau$. A possible estimate for τ is $|\alpha_1|/\mu$; in this case we obtain the same capillary number as in the Newtonian case. It might be argued, however, that shorter relaxation times could be important. Using such shorter relaxation times for τ would also raise the value of Ca.

4. Numerical results

In this section, we present numerical results that show the formation of a singularity in a free surface for a model problem. The results are computed with the Fluid Dynamics Package (FIDAP) Version 4.0, which uses the finite element method (cf. Engelman and Sani [1986]). The computed free surfaces first appear to have a corner, but as time evolves, this corner sharpens and looks more like a cusp. Unfortunately, the solution becomes polluted by wiggles at this point; we shall explain the suspected reasons for this below. The numerical method is clearly not capable of resolving the details of the flow near the singularity; however, we observe that the development of a singularity and the time at which it develops persist under mesh refinement. We believe that the appearance of the singularity in the computations corresponds physically to the development of a cusp as observed in the experiments discussed above.

Figure 18. Flow domain for numerical simulations.

The computational domain at time zero is a unit square in the x-y plane, as shown in Figure 18. The top boundary at $y=1$, $0\le x\le 1$, is a free surface. Along the upper parts of the vertical sides ($x=0$, $0.8\le y\le 1$ and $x=1$, $0.8\le y\le 1$), the boundary condition is zero vertical velocity and the horizontal velocity is half of a parabolic velocity profile. The latter has a maximum value of unity at $y=1$. The boundary along $0\le y\le 0.8$ at $x=0$ and 1, and along $0\le x\le 0.3$ at $y=0$, and

$0.7 \leq x \leq 1.0$ at $y=0$ is a solid wall. Along $0.3 \leq x \leq 0.7$ at $y=0$, the horizontal velocity is zero and the normal traction is 1, so that there is a negative pressure sucking the fluid out. The viscosity and density of the fluid are prescribed to be unity. The surface tension is varied, as described below.

A mixed velocity pressure formulation is used. Interior elements are nine-node isoparametric quadrilaterals with biquadratic velocity and discontinuous linear pressure functions. Three-node quadratic elements are used on the free surface.

An initial velocity field is computed by solving the Stokes problem with the position of the free surface kept fixed. The transient problem is then computed with the implicit backward Euler integration scheme. At each time-step, the Newton-Raphson scheme is used with a relaxation constant of 0.5. The initial timestep is 0.01, and thereafter, a variable time increment is selected automatically by the code.

We present results for various values of the surface tension. Figure 19 displays the formation of a cusp for zero surface tension. The mesh size is 21 by 17, and the mesh is displayed in each plot. There are 357 nodes, 80 interior elements and 10 elements on the free surface. The times shown on the plots are 0.02, 0.89, 2.11, 3.78, 5.60 and 7.45. The cusp has started to form by time 3.78. The velocity vector plots for times 0.01 and 3.78 are shown in Figure 20 and 21, respectively.

After the formation of the cusp, wiggles appear in the free surface. We believe that this is due to improper handling of the kinematic free surface condition. At a cusp, the kinematic free surface condition must be suspended; fluid particles can move from the free surface into the interior. The code, however, does not know this. The computed results past the development of the cusp can therefore not be trusted.

When surface tension is 0.1, the cusp does not form. Instead, a steady state is attained, with a smooth curve at the free surface. Figure 22 shows the evolution of the mesh at time 0.02, 0.82, 1.89, 3.66, 6.66, 11.57, 19.10, 28.91, 40.31, 53.53, 69.30 and 88.80. By the latter time, a steady state has been reached. The velocity vector plot at time 88.80 is shown in Figure 23. If a

much larger amount of surface tension is present (e.g., 1.0), the free surface does not move appreciably from its initial position, and a cusp does not form.

The evolution of the free surface for surface tension 0.05 is shown in Figure 24, where the times are 0.02, 0.86, 2.17, 4.27, 7.52, 12.01, 17.58, 21.01 and 27.2. A cusp starts to form by time 12.01. The velocity vector plot for time 21.01 is shown in Figure 25. At later times, a steady state is reached. These computations have been convergence tested on a finer mesh.

The numerical results of this section show the formation of a cusp in slow viscous flow, for values of the surface tension that are in the order-of-magnitude range observed in the experiments described in the earlier sections.

The numerical study of Lister [1989] of selective axisymmetric withdrawal into a sink from a stratified viscous two-layer system is similar to the problem studied here. He finds that below a critical value of surface tension, the free surface is drawn out into a thin filament stretching toward the sink.

5. Conclusions and Discussion

1. It is easy to create two-dimensional cusped surfaces at liquid-air interfaces.

2. In all cases studied by us, the formation of cusped surfaces between air and liquid occurred for all non-Newtonian liquids and for some Newtonian liquids. Our criterion to judge whether a fluid is non-Newtonian is that a non-Newtonian fluid will climb a rod.

3. The formation of cusps is a critical phenomenon; other things being equal, the interface is rounded for small values of the streaming speed and becomes cusped at a critical speed and beyond. In non-Newtonian fluids this critical speed is very distinct; in Newtonian fluids it is less distinct and the change from a rounded to a pointed interface appears to be gradual.

4. Cusping is unusual at the interface of two liquids. Higher viscosity liquids in water form rollers, which are replaced by fingering flows when the viscosity of the liquid on the cylinder is too low to support a roller.

5. SAE 30 motor oil and water support a cusped interface with periodic scallops along the cusp which form sites for the fingering of water into oil. The motor oil is Newtonian and will not cusp in air.

6. We have given a local analysis of the Stokes equations near a cusp. For zero surface tension, this local analysis yields an interface of the form $y^2 = -cx^3$. A small surface tension would change the exponents and, more seriously, it leads to a point force at the cusp which has to be balanced by a singularity of the flow. This leads to Richardson's solution, which has an infinite backward velocity at the cusp and an infinite rate of energy dissipation. However, we estimate that for the situations on which cusps are actually observed, Richardson's solution would not become dominant until molecular length scales are reached. At such length scales, one would have to modify the physics.

7. Linear viscoelasticity would predict stresses at a cusp which are less singular than in the Newtonian case. However, it seems likely that nonlinear extensional behavior of non-Newtonian fluids is quite important. Experimentally, non-Newtonian fluids form cusps at lower speeds than Newtonian fluids. A qualitative explanation may be that cusping avoids the stagnation point inevitably present on a smooth interface and thus relieves extensional stresses.

8. Numerical simulations show results which are in qualitative agreement with the experiments; cusps form for low values of surface tension, while a steady smooth interface is reached at higher values.

Acknowledgements

The work of D.D. Joseph and J. Nelson was supported by the NSF, the Army Research Office, Mathematics and AHPCRC at the University of Minnesota, and the Department of Energy. M. and Y. Renardy were supported by the NSF under Grants DMS-8796241 and DMS-8902166, respectively.

REFERENCES

Acrivos, A. and Lo, T.S. 1978 Deformation and breakup of a single slender drop in an extensional flow. *J. Fluid Mech.* **86**, 641–672.

Astarita, G. and Apuzzo, G. 1965 Motion of gas bubbles in non-Newtonian liquids. *A. I. Ch. E. Jl.* **11**, 815–820.

Barnett, S.M., Humphrey, A.E. and Litt, M. 1966 Bubble motion and mass transfer in non-Newtonian fluids. *A. I. Ch. E. Jl.* **12**, 253–259.

Buckmaster, J.D. 1972 Pointed bubbles in slow viscous flow. *J. Fluid Mech.* **55**, 385–400.

Buckmaster, J.D. 1973 The bursting of pointed drops in slow viscous flow. *ASME J. Appl. Mech.* **40**, 18–24.

Calderbank, P.H. 1967 Review Series No. 3—Gas absorption from bubbles. *Trans. Instn. Chem. Engrs.* **45**, 209–220.

Calderbank, P.H., Johnson, D.S. and Loudon, J. 1970 Mechanics and mass transfer of single bubbles in free rise through some Newtonian and non-Newtonian liquids.*Chem. Engng. Sci.* **25**, 235–256.

Davies, A.R. 1988 Reentrant corner singularities in non-Newtonian flow. Part I. Theory. *J. Non-Newtonian Fluid Mech.* **29**, 269–293.

De Gennes, P.G. 1985 Wetting: static and dynamics. *Rev. of Mod. Phys.* **57**, 827–863.

Dean, W.R. and Montagnon, P.E. 1949 On the steady motion of viscous liquid in a corner. *Proc. Cambridge Phil. Soc.* **45**, 389–394.

Dussan, V.E. 1976 The moving contact line: the slip boundary condition. *J. Fluid Mech.* **77**, 665–684.

Engelman, M.S. and Sani, R.I. 1986 Finite element simulation of incompressible fluid flows with a free/moving surface. In: Taylor, C., Johnson, J.A. and Smith, W.R. (eds.), *Computational Techniques for Fluid Flow,* 47–74. Pineridge Press, Swansea.

Grace, J.P. 1971 Dispersion phenomena in high viscosity immiscible fluid systems and application of static mixers as dispersion devices in such systems. *Engng. Found. 3rd Res. Cong. Mixing.* Andover, New Hampshire.

Hassager, O. 1985 The motion of viscoelastic fluids around spheres and bubbles. In: Lodge, A.S., Renardy, M. and Nohel, J.A. (eds.), *Viscoelasticity and Rheology,* 1–11. Academic Press, Orlando.

Hinch, E.J. and Acrivos, A. 1979 Steady long slender droplets in two-dimensional straining motion. *J. Fluid Mech.* **91**, 401–414.

Huh, C. and Scriven, L.E. 1971 Hydrodynamic model of steady movement of a solid/liquid/fluid contact line. *J. Colloid Interface Sci.* **35**, 85–101.

Joseph, D.D., Nguyen, K. and Beavers, G.S. 1984 Non-uniqueness and stability of the configuration of flow of immiscible fluids with different viscosities. *J. Fluid Mech.* **141**, 319–345.

Koplik, J., Banavar, J.R. and Willemsen, J.F. 1988 Molecular dynamics of Poiseuille flow and moving contact lines. *Phys. Rev. Letters* **60**, 1282–1285.

Lamb, H. 1932 Hydrodynamics. Dover Publications, New York.

Leal, L.G., Skoog, J. and Acrivos, A. 1971 On the motion of gas bubbles in a viscoelastic liquid. *Can. J. Chem. Engng.* **49**, 569–575.

Lister, J.R. 1989 Selective withdrawal from a viscous two-layer system. *J. Fluid Mech.* **198**, 231–254.

Mhatre, M.V. and Kintner, R.C. 1959 Fall of liquids drops through pseudoplastic liquids. *Ind. Engng. Chem.* **51**, 865–867.

Michael, H.D. 1958 The separation of a viscous liquid at a straight edge. *Mathematika* **5**, 82–84.

Philippoff, W. 1937 The viscosity characteristics of rubber solutions.. *Rubb. Chem. Technol.* **10**, 76–104.

Rallison, J.M. and Acrivos, A. 1978 A numerical study of the deformation and burst of a viscous drop in an extensional flow. *J. Fluid Mech.* **89**, 191–200.

Rayleigh, Lord 1890 On the theory of surface forces. *Phil. Mag., 5th ser.* **34**, 285–298 and 456–475.

Richardson, S. 1968 Two dimensional bubbles in slow flow. *J. Fluid Mech.* **33**, 475–493.

Rumscheidt, F.D. and Mason, S.G. 1961 Particle motion in sheared suspensions. XII. Deformation and burst of fluid drops in shear and hyperbolic flow. *J. Colloid. Sci.* **16**, 238–261.

Sherwood, J.D. 1981 Spindle shaped drops in a viscous extensional flow. *Math. Proc. Camb. Phil. Soc.* **90**, 529–536.

Taylor, G.I. 1934 The formation of emulsions in definable fields of flow. *Proc. Roy. Soc.* A **146**, 501–523.

Taylor, G.I. 1964 Conical free surfaces and fluid interfaces. *Proc. 11th Int. Cong. Appl. Mech.*, Munich.

Thompson, P.A. and Robbins, M.O. 1989 Simulations of contact-line motion: slip and the dynamics of contact. *Phys. Rev. Letts.* **63**, 766–769.

Warshay, M.E., Bogusz, E., Johnson, M. and Kintner, R.C. 1959 Ultimate velocity of drops in stationary liquid media. *Can. J. Chem. Engng.* **37**, 29–36.

Zana, E. and Leal, L.G. 1978 The dynamics and dissolution of gas bubbles in a viscoelastic fluid. *Int. J. Multiphase Flow* **4**, 237–262.

LIST OF FIGURES

Figure 12 Scale for 64∞ magnification of cusp tip in figures 13, 14, and 15 using a Nikon microscope. Each bar is 0.001 inch; 0.040 inches altogether.

Figure 13 Critical speed for cusping of STP is approximately 2.9 RPM. a) 2 RPM, the bump on the rounded end is an air bubble emerging through the interface, b) 24 RPM.

Figure 14 The critical speed for 500 cs. silicone oil is approximately 75 RPM. a) 44 RPM, b) 75 RPM.

Figure 15 The critical rotation speed for castor oil is approximately 113 RPM. a) 67 RPM, b) 122 RPM.

Figure 16 Comparison of the measured values (dots) of the cusp tip with $y=-cx^{3/2}$(lines). a) STP, c=.4, b) 500 cs silicone oil, c=.33, c) castor oil, c=.29. The value of c is chosen to fit data points close to the cusp point. Larger values of c open the cusp. This type of comparison between theory and experiment is only qualitative since we don't know the values of x for which the higher order corrections become important. The higher order corrections would be a composition of symmetric and antisymmetric functions like (3) and (9) in a combination determined globally.

Figure 19 The top boundary is a free surface. Fluid flows in through the upper parts $0.8\le y\le 1$ of the side boundaries and flows out through the middle part $0.3\le x\le 0.7$ of the bottom boundary. The free surface evolves into a cusp. Surface tension is zero. Times of free surface evolution are indicated below each figure.

Figure 20 The top boundary is a free surface. This is a velocity vector plot close to the initial time for the flow in figure 19. Surface tension is zero. Time is 0.01.

Figure 21 The top boundary is a free surface. This is a velocity vector plot for the flow in figure 19 at a time when a cusp is forming. Surface tension is zero. Time is 3.78.

Figure 22 The top boundary is a free surface. The flow conditions are the same as those of figure 19, except for the presence of a sufficiently large surface tension that keeps the free surface smooth. The evolution of the flow is shown. Surface tension is 0.1. Times of free surface evolution are shown below each figure.

Figure 23 The final plot of figure 22 is shown here as a velocity vector plot, showing that the free surface is smooth. Surface tension is 0.1. Time is 88.80.

Figure 24 The evolution of the flow of figure 19 with the addition of half the amount of surface tension present in the flow of figure 22 is shown. A cusp forms. Surface tension is 0.05. Times of free surface evolution are shown below each figure.

Figure 25 The velocity vector plot for the onset of cusp formation in the flow shown in figure 24 is displayed. Surface tension is 0.05. Time is 21.01.

(a)

(b)

Figure 3 Cylinder coated with 12,500 cs silicone oil cusps in air. a) liquid is dragged down between the cylinders, b) liquid is dragged up between cylinders.

Figure 4 Cusp point on the 12,500 cs silicone oil as seen through a Nikon microscope.

Figure 5. Cylinder coated with STP (polyisobutylene in petroleum oil) cusps in air. The liquid is dragged down between the cylinders.

(a)

(b)

Figure 6 Cylinder coated with M1 (polyisobutylene in kerosene and polybutene) cusps in air. a) 19 RPM, b) 75 RPM. At 75 RPM a ribbing instability has developed. The cusped interface has developed scallops.

(a)

(b)

Figure 7 Low molecular weight silicone oils do not cusp at 200 RPM. a) 500 cs is marginal, but a Nikon microscope shows it does cusp. b) 200 cs silicone oil does not cusp at 200 RPM.

(a)

(b)

Figure 8. The critical speed for SAE 30 motor oil and water is approximately 51 RPM. a) 43 RPM, b) 75 RPM.

(a)

(b)

Figure 9 Critical speed for cusping of M1 in air is approximately 2.4 RPM. a) 2 RPM, b) 75 RPM (cf. Figure 7).

(a)

(b)

Figure 10 Critical speed for cusping of 2% aqueous polyox in air is approximately 0.75 RPM. a) 0.7 RPM, b) 27 RPM.

(a)

(b)

Figure 11 Critical speed for cusping of 1% aqueous polyox in air is 51.7 RPM. a) 27 RPM, b) 75 RPM.

Figure 12 Scale for 64∞ magnification of cusp tip in figures 13, 14, and 15 using a Nikon microscope. Each bar is 0.001 inch; 0.040 inches altogether.

(a)

(b)

Figure 13 Critical speed for cusping of STP is approximately 2.9 RPM. a) 2 RPM, the bump on the rounded end is an air bubble emerging through the interface, b) 24 RPM.

(a)

(b)

Figure 14 The critical speed for 500 cs. silicone oil is approximately 75 RPM. a) 44 RPM, b) 75 RPM.

(a)

(b)

Figure 15 The critical rotation speed for castor oil is approximately 113 RPM. a) 67 RPM, b) 122 RPM.

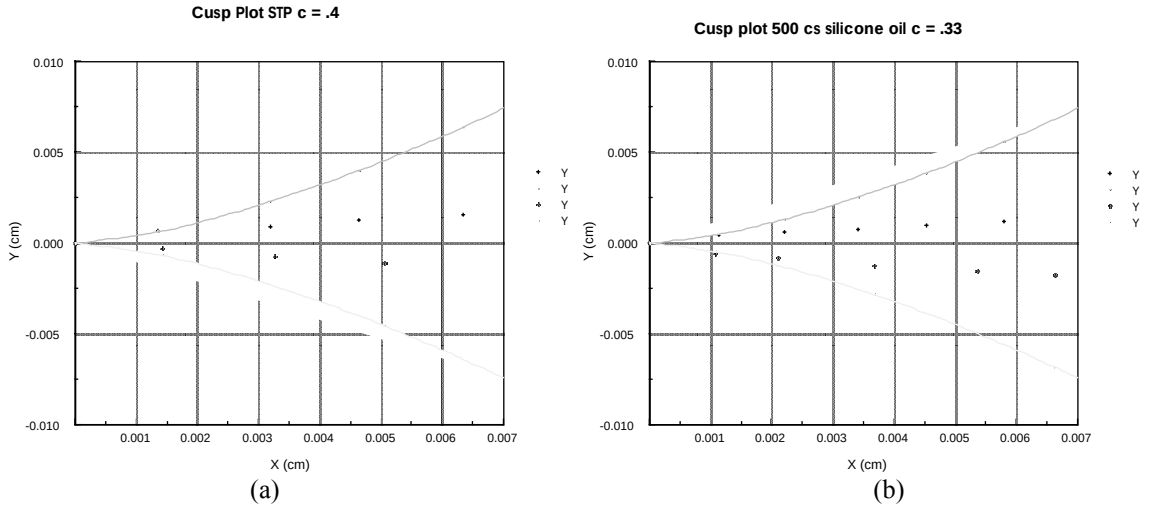

(a)

(b)

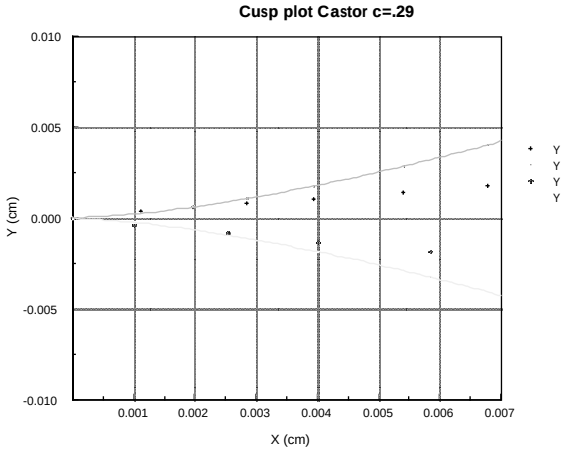

(c)

Figure 16 Comparison of the measured values (dots) of the cusp tip with $y=-cx^{3/2}$(lines). a) STP, c=.4, b) 500 cs silicone oil, c=.33, c) castor oil, c=.29. The value of c is chosen to fit data points close to the cusp point. Larger values of c open the cusp. This type of comparison between theory and experiment is only qualitative since we don't know the values of x for which the higher order corrections become important. The higher order corrections would be a composition of symmetric and antisymmetric functions like (3) and (9) in a combination determined globally.

Figure 19 The top boundary is a free surface. Fluid flows in through the upper parts $0.8\le y\le 1$ of the side boundaries and flows out through the middle part $0.3\le x\le 0.7$ of the bottom boundary. The free surface evolves into a cusp. Surface tension is zero. Times of free surface evolution are indicated below each figure.

Figure 20 The top boundary is a free surface. This is a velocity vector plot close to the initial time for the flow in figure 19. Surface tension is zero. Time is 0.01.

Figure 21 The top boundary is a free surface. This is a velocity vector plot for the flow in figure 19 at a time when a cusp is forming. Surface tension is zero. Time is 3.78.

Figure 22 The top boundary is a free surface. The flow conditions are the same as those of figure 19, except for the presence of a sufficiently large surface tension that keeps the free surface smooth. The evolution of the flow is shown. Surface tension is 0.1. Times of free surface evolution are shown below each figure.

Figure 23 The final plot of figure 22 is shown here as a velocity vector plot, showing that the free surface is smooth. Surface tension is 0.1. Time is 88.80.

Figure 24 The evolution of the flow of figure 19 with the addition of half the amount of surface tension present in the flow of figure 22 is shown. A cusp forms. Surface tension is 0.05. Times of free surface evolution are shown below each figure.

Figure 25 The velocity vector plot for the onset of cusp formation in the flow shown in figure 24 is displayed. Surface tension is 0.05. Time is 21.01.